



UNICA

UNIVERSITÀ
DEGLI STUDI
DI CAGLIARI



Università di Cagliari

UNICA IRIS Institutional Research Information System

This is the *accepted* manuscript version of the following contribution:

O. Assila, Z. Bencheqroun, E. Rombi, T. Valente, A.S. Braga, H. Zaitan, A. Kherbeche, O. S.G.P. Soares, M.F.R. Pereira, A.M. Fonseca, P. Parpot, Isabel C. Neves, Raw clays from Morocco for degradation of pollutants by Fenton-like reaction for water treatment, *Colloids and Surfaces A: Physicochemical and Engineering Aspects*, 679, 2023, 132630

The publisher's version is available at:

<http://dx.doi.org/10.1016/j.colsurfa.2023.132630>

When citing, please refer to the published version.

1 **Raw clays from Morocco for degradation of pollutants**

2 **by Fenton-like reaction for water treatment**

3
4 O. Assila^{1,2}, Z. Bencheqroun^{1,3}, E. Rombi⁴, T. Valente⁵, A.S. Braga⁵, H. Zaitan³, A.
5 Kherbeche², O.S.G.P. Soares^{6,7}, M.F.R. Pereira^{6,7}, A.M. Fonseca^{1,8}, P. Parpot^{1,8}, I.C.
6 Neves^{1,8,*}

7
8 ¹*CQUM, Centre of Chemistry, Chemistry Department, University of Minho, Campus de*
9 *Gualtar, 4710-057, Braga, Portugal*

10 ²*Laboratory of Catalysis, Process, Materials and Environment, School of Technology,*
11 *University Sidi Mohammed Ben Abdellah Fez, Morocco*

12 ³*Processes, Materials, Environment Laboratory (LPME), Department of Chemistry,*
13 *Faculty of Sciences and Technology, Sidi Mohamed Ben Abdellah University, Fez, BP.*
14 *2202, Morocco*

15 ⁴*Dipartimento di Scienze Chimiche e Geologiche, University of Cagliari, Complesso*
16 *Universitario di Monserrato, 09042 Monserrato, Italy*

17 ⁵*ICT, Institute of Earth Sciences, Pole of the University of Minho, 4710-057 Braga,*
18 *Portugal*

19 ⁶*LSRE-LCM - Laboratory of Separation and Reaction Engineering – Laboratory of*
20 *Catalysis and Materials, Faculty of Engineering, University of Porto, Portugal*

21 ⁷*ALiCE - Associate Laboratory in Chemical Engineering, Faculty of Engineering,*
22 *University of Porto, Portugal*

23 ⁸*CEB - Centre of Biological Engineering, University of Minho, Campus de Gualtar,*
24 *4710-057 Braga, Portugal*

25 **Abstract**

26 Three raw clays from Morocco were used as heterogeneous catalysts for Fenton-like
27 oxidation of organic pollutants in water. The selected pollutants were two dyes used in
28 the textile industry, Congo Red (CR) and Tartrazine (Tar, known also as a food coloring
29 compound, E102) and Caffeine (Caf), a stimulant drug present in popular beverages such
30 as coffee and tea, commonly used in Morocco. Two different processes were used for
31 their degradation: (i) Fenton-like reaction; and (ii) electro-Fenton-like reaction. Process
32 (i) was used for Tar and Caf degradation in the presence of clays from different region of
33 Morocco (Middle Atlas - Clay_{MA}, Fez - Clay_F, and Ourika - Clay_O), the best results being
34 obtained with Clay_O and Clay_{MA}, on which 60.0 and 23.4 % of conversion and 41.0 and
35 20.5 % of mineralization were achieved for Tar and Caf, respectively. Process (ii) was
36 used for degrading CR by clay-modified electrodes (CME) using the rawclays from Fez
37 and Ourika regions (Clay_F and Clay_O). The stability of the CME was assessed by cyclic
38 voltammetry studies, which proved that they are stable in the experimental conditions
39 used. The electrodegradation of CR dye, performed without hydrogen peroxide in the
40 reaction medium, achieve 67.0 % of mineralization at the end of electrolysis (2 h).

41

42 **1. Introduction**

43 The 2030 Agenda for Sustainable Development with its 17 sustainable development goals
44 (SDGs) from the United Nations (UN) aims to end poverty, conserve biodiversity, combat
45 climate change and improve the livelihoods of people everywhere (Axon and James,
46 2018; United Nations, 2016). In the 17 SDGs, water and the use of raw materials are
47 interlinked, and chemistry and geochemistry are two of the keys to achieve these goals in
48 order to preserve society and the planet for the future generations (Anastas and
49 Zimmerman, 2016; United Nations, 2023). Moroccan raw clays were utilized as

50 heterogeneous catalysts to eliminate pollutants from effluents in order to tackle the issue
51 of clean water through the valorization of raw materials via the oxidation Fenton reaction.
52 Morocco is a country with important deposits of clays and these geological materials are
53 very attractive to apply as adsorbents (Bencheqroun et al., 2019a) or heterogeneous
54 catalysts for Fenton-like oxidation (Assila et al., 2023a).

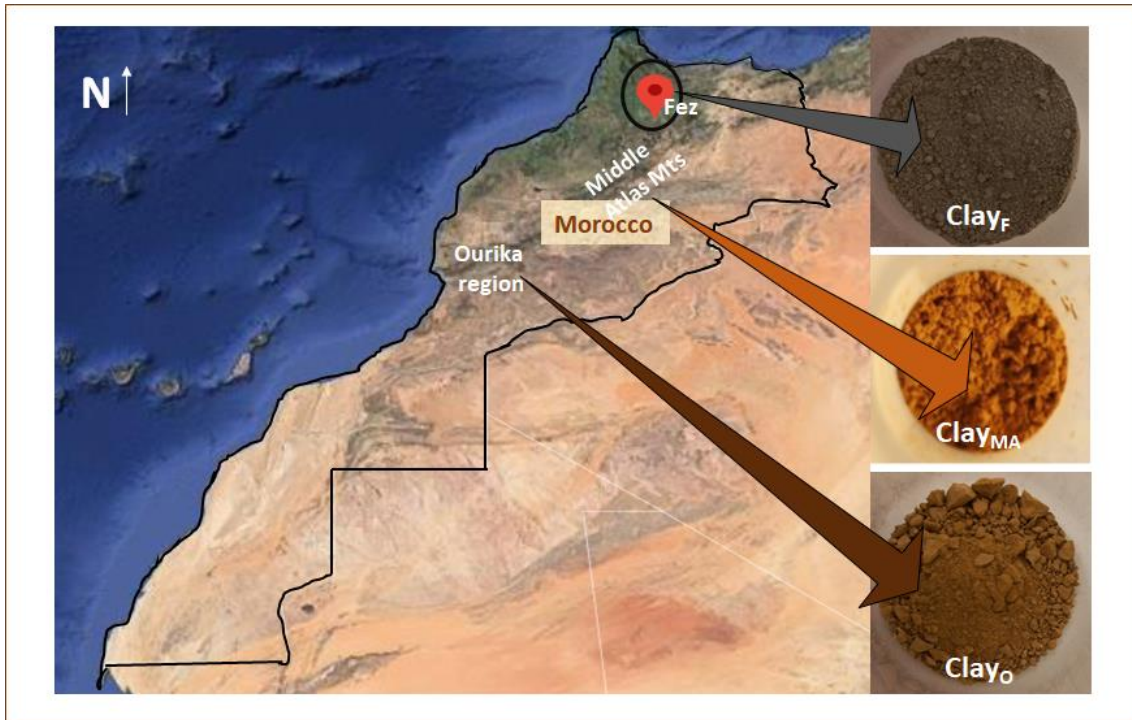
55 Porous materials as clays offer a word of possibilities for preparing heterogeneous
56 catalysts due to their stability in different pH ranges, easily separation, and reutilization.
57 Several examples were find in literature using the clays as heterogeneous catalysts (Aid
58 et al., 2017; Hadjltaief et al., 2019; Herney-Ramirez et al., 2010). The degradation of
59 reactive blue 19 was performed by TiO₂-coated Tunisian clay synthesized by
60 impregnation method, and the high photodegradation of dye by TiO₂-clay is due to the
61 anatase phase stability of the photocatalyst (Hadjltaief et al., 2019). Montmorillonite clay
62 combined with bentonite, acid-washed clay (K10), and Al-pillared clay underwent ion
63 exchange with nickel for the purpose of ethylene oligomerization in a fixed-bed flow
64 reactor, demonstrating good activity and stability (Aid et al., 2017). In the work of Jesus
65 et al. (2022), a natural clay was using as a support for magnetite and copper-containing
66 magnetite for heterogeneous Fenton/photo-Fenton degradation of antibiotics in
67 wastewater treatment plants effluent.

68 Clays are a group of minerals used as raw materials in the ceramic, paper, and metal
69 industries, in the field of pets feeding, and as adsorbents, discoloration agents, ion
70 exchanger and supports (Aid et al., 2017; Antonielli et al., 2020; Haciosmanoglu et al.,
71 2022; Maryan et al., 2015). These minerals are phyllosilicates with basic building blocks
72 of Si(O, OH)₄ tetrahedra and M(O, OH)₆ octahedra, and mostly M = Al³⁺, Mg²⁺ or Fe^{2+,3+}
73 (Assila et al., 2023a; Bencheqroun et al., 2019a; Schoonheydt, 1991).

74 Fenton-like oxidation reaction is very attractive, non-toxic nature, ease to use, and low
75 cost (Fida et al., 2017; Fu et al., 2022; Liu et al., 2021, **Usman et al., 2023**; Wang and
76 Tang, 2021). However, there are few examples using clays as modified electrodes for
77 degradation of pollutants by electro Fenton-like oxidation. Electrochemistry is one of the
78 sustainable methods to be used for the treatment of waste effluents; indeed, it does not
79 require high temperatures, allows the achievement of high degrees of mineralization of
80 the pollutants, and has low operational costs (Brillas et al., 2009; Chaplin, 2014). A
81 further advantage comes from the possibility of carrying out the electrochemical process
82 using electrodes modified with heterogeneous catalysts, due to their peculiar properties
83 (Poza-Nogueiras et al., 2018).

84 The works of Ozcan *et al.* (2017) showed that iron in the kaolin clay is capable to degrade
85 the emerging pollutant enoxacin with a TOC of 98 % after 7 h of reaction. Methylene
86 blue was also degraded with the clay modified electrode with a **chemical oxygen demand**
87 **(COD)** of 96.5% after 45 min of reaction (Ma et al., 2009). Modified electrodes using
88 iron oxide supported on nanostructured allophane clays, with both Fe^{3+} and Fe^{2+} species
89 on the surface, were used for degrading atrazine with higher efficiency compared to the
90 heterogeneous Fenton-like catalysis (Garrido-Ramírez et al., 2013). **The clay modified**
91 **electrodes (CME)** combine the advantages of the catalytic properties of the clay structures
92 with the versatility, energy efficiency, cost effectiveness, and facility for process
93 automation of the electrochemical processes (Herney-Ramirez et al., 2010).

94 Herein we report the degradation of different pollutants by Fenton-like reaction and
95 electro Fenton-like oxidation using several raw clay minerals from Morocco. The places
96 where the clays come from cover an important part of Morocco territory (Fig. 1), which
97 confirms the presence of huge deposits of clay minerals in this country.



98

99 **Fig. 1.** Map of Morocco showing the location of the clays sites.

100

101 Two clays were collected from the Ourika region (Clay_O) and the city of Fez (Clay_F),
 102 while one sample was collected from the Middle Atlas region (Clay_{MA}). They were used
 103 for studying the degradation of three different organic pollutants in water. Tartrazine (Tar)
 104 and caffeine (Caf) were removed by Fenton-like reaction using the three raw clays,
 105 whereas Congo Red (CR) was degraded by electro Fenton-like oxidation using CME
 106 based on Clay_O and Clay_F.

107 **2. Experimental section**

108 **2.1. Preparation and characterization of the heterogeneous clay catalysts**

109 Three raw clays from Morocco obtained from deposits located in the Middle Atlas region
 110 (Clay_{MA}, where MA stands for Middle Atlas), the city of Fez (Clay_F, where F stands for
 111 Fez), and the Ourika region (Clay_O, where O stands for Ourika) were used in this study
 112 without any prior activation. Samples were ground, sieved to obtain particle sizes (60 -

113 100 μm), and washed with distilled water. After that, all clays were dried at 60 °C for 24 h
114 and stored in hermetic plastic bottles until further use.

115 **In order to study the effect of the presence of the metal in the clay**, heterogeneous clay
116 catalysts were prepared by addition of zinc or copper using an adapted method described
117 in (Assila et al., 2023). **Typically**, aqueous solutions (250 mL) **containing 2.70×10^{-2} mmol**
118 **of Cu or Zn** were mixed with 4 g of the pristine support (Clay_{MA}) at pH 4.0. The
119 suspensions were stirred during 24 h at room temperature. After each ion-exchange step,
120 the suspensions were filtered-off, washed with deionized water and dried at 60 °C
121 overnight. Finally, the solids were calcined at 350 °C during 4 h under a dry-air stream.
122 The samples were identified as $\text{Cu-Clay}_{\text{MA}}$ and $\text{Zn-Clay}_{\text{MA}}$. All clay samples were used
123 as heterogeneous catalysts for the degradation of tartrazine (Tar, $\text{C}_{16}\text{H}_9\text{N}_4\text{Na}_3\text{O}_9\text{S}_2 \geq 90\%$,
124 Sigma-Aldrich) and caffeine (Caf, $\text{C}_8\text{H}_{10}\text{N}_4\text{O}_2 \geq 99\%$, Sigma-Aldrich) in Fenton-like
125 reaction. In addition, Clay_{F} and Clay_{O} were used for preparing clay modified electrodes
126 (CME) for the degradation of Congo Red (CR, $\text{C}_{32}\text{H}_{22}\text{N}_6\text{Na}_2\text{O}_6\text{S}_2$, 3,3'-([1,1'-biphenyl]-
127 4,4'-diyl)bis(4-aminonaphthalene-1-sulfonic acid, Sigma-Aldrich) by electro Fenton-like
128 oxidation.

129 The heterogeneous clay catalysts were characterized by different techniques, such as
130 powder X-ray diffraction (XRD), X-ray photoelectron spectroscopy (XPS), N_2
131 adsorption, scanning electron microscopy coupled with energy dispersive X-ray analysis
132 (SEM/EDX), and chemical analysis.

133 Mineralogical identification was performed by XRD through a Philips X'pert Pro-MPD
134 diffractometer (Philips PW 1710, APD), provided with an automatic divergence slit and
135 a graphite monochromator, using $\text{CuK}\alpha$ radiation powdered at 40 kV and 40 mA ($\text{CuK}\alpha_1$
136 = 1.54060 Å and $\text{CuK}\alpha_2$ = 1.54443 Å). The XRD patterns were obtained from powders
137 (bulk sample) and from oriented aggregates ($< 2 \mu\text{m}$), in the range of 2θ from 3 to 65°

138 and 3 to 35°, respectively, with a step size of 0.02° and a counting time of 1.25 s. Sample
139 preparation for XRD analysis involved gentle grinding of the solid into a fine powder and
140 packing of approximately 1.0 g of the sample into the sample holder. Identification of
141 clay minerals was obtained in the oriented aggregates after chemical and thermal
142 treatments (ethylene glycol saturation and heating at 490 °C).

143 XPS analysis was performed by recording the high-resolution and survey spectra with a
144 Kratos Axis-Supra instrument. Monochromatic X-ray source Al K α (1486.6 eV) was used
145 for all samples and experiments. The residual vacuum in the X-ray analysis chamber was
146 maintained at around 7.2×10^{-9} torr. The samples were fixed to the sample holder with
147 double sided carbon tape. Due to the non-conducting nature of the samples, it was
148 necessary to use a co-axial electron neutralizer to minimize surface charging, which
149 performed the neutralization by itself. Charge referencing was done by setting the binding
150 energy of C1s photo peak at 285.0 eV C 1s hydrocarbon peak. Photoelectrons were
151 collected from a take-off angle of 90° relative to the sample surface. The measurement
152 was done in a Constant Analyser Energy mode (CAE) with a 10 mA of emission current
153 and 160 eV pass energy for survey spectra and 20 eV pass energy for high resolution
154 spectra. A wide scan survey spectrum was used to identify and quantify the elements in
155 the sample. High-resolution narrow scans are used to build the chemical state assessment,
156 as well as to quantify the presence of the reference elements in each sample. Data analysis
157 and atomic quantification were determined from the XPS peak areas using the ESCApe
158 software supplied by the manufacturer Kratos Analytical.

159 Nitrogen (N₂) adsorption-desorption isotherms were measured at -196 °C on ASAP2040
160 Micrometrics device endowed with a thermal conductivity detector. The prepared
161 samples were previously degassed at 90 °C for 1 h and then at 250 °C with a heating rate
162 of 5 °C min⁻¹ for 6 h, up to a residual pressure smaller than 0.5 Pa. The specific surface

163 area and pore size distribution (PSD) were determined by the Brunauer-Emmett-Teller
164 (BET) method and Barret-Joyner-Halenda (BJH) analysis, respectively, using the
165 adsorption branch.

166 SEM/EDX analysis was performed on a Phenom ProX with EDS detector (Phenom-
167 World BV, Netherlands). All data were acquired using the ProSuite software integrated
168 with Phenom Element Identification software, allowing the quantification of the
169 concentration of the elements present in the samples, expressed in either weight or atomic
170 percentages. The samples were added to aluminum pin stubs with electrically conductive
171 carbon adhesive tape (PELCO Tabs™) and were imaged without coating. The aluminum
172 pin stub was then placed inside a Phenom Charge Reduction Sample Holder (CHR), and
173 different points were analyzed for elemental composition. EDS analysis was conducted
174 at 15 kV with intensity map.

175 Chemical analysis was performed by inductively coupled plasma optical emission
176 spectroscopy (ICP-OES) for the quantification of metals in the liquid phase during the
177 ion-exchange process using an Optima 8000 spectrometer (PerkinElmer). A 5110
178 ICP-OES spectrometer (Agilent Technologies) was instead used to quantify the metals in
179 the solid samples.

180

181 **2.2 Fenton-like oxidation**

182 For the degradation of Tar or Caf with the different heterogeneous clay catalysts, the
183 concentration of pollutant (30 ppm), temperature (40 °C), and pH (=3.0) were fixed at the
184 best values found in a preliminary study in a stirred semi-batch reactor at atmospheric
185 pressure using Clay_{MA} as catalyst (Assila et al., 2023a). Prior to experiments, all catalysts
186 were pretreated at 100 °C for 2 h in an oven. The semi-batch reactor was loaded with 250
187 mL of a solution of pollutant prepared with ultrapure water produced with an ultrapure

188 water system (Milli-Q, EQ 7000), using 200 mg of catalyst and 5 mL of H₂O₂ (12 mM).
189 The reaction was then performed under stirring at 300 rpm, during 300 min. Sampling
190 was carried out at fixed time intervals and the reaction was stopped with the addition of
191 an excess of sodium sulphite (Na₂SO₃, Sigma-Aldrich), which instantaneously consumes
192 the unreacted H₂O₂. Catalytic tests were performed in duplicate, and the maximum
193 deviation observed in the removal of the organic pollutants was 2%. **The stability of the**
194 **best clay, Clay_O, for Tar degradation was studied using the experimental catalytic**
195 **conditions determined above. Two cycles were performed and for each cycle, the used**
196 **catalyst was filtered-off, washed with ethanol, and dried in an oven at 70 °C overnight**
197 **before reutilization. The solution recovered after each catalytic test was analyzed by ICP-**
198 **OES to quantify the amount of the metal species eventually leached during reaction.**

199

200 **2.3 Electro Fenton-like oxidation**

201 Clays modified electrodes (CME) were prepared using Clay_F and Clay_O by the procedure
202 already described in previous papers (Assila et al., 2023a; Ferreira et al., 2018). Typically,
203 CME were prepared by dispersing 20 mg of the clays powders in a mixture of 180 μL
204 ultrapure water (Barnsted E-pure system, 18.2 MΩ cm at 20 °C) and 180 μL Nafion®
205 suspension (5 wt. %, Sigma-Aldrich). The resulting suspensions were homogenized using
206 an ultrasound bath and totally deposited onto the wet proofed Carbon Toray paper (CT,
207 geometrical area of 4.0 cm², Quintech); the solvent was then evaporated at room
208 temperature overnight. CT paper was glued to the platinum wire using a conductive
209 carbon cement (Quintech) and subsequently dried at room temperature during 24 h.

210 **A three-electrodes cell assembly composed of the reference electrode, consisting of a**
211 **saturated calomel electrode (SCE) Hg/Hg₂Cl₂ (KCl sat.) separated from the solution by a**
212 **Haber-Luggin capillary tip, a platinum foil (99, 95%) as a counter electrode, and a CME**

213 **working electrode, was used for electrochemical measurements.** The electrochemical
214 instrumentation consisted of a potentiostat/galvanostat from Amel Instruments coupled
215 to a microcomputer (Pentium II/ 500 MHz) through an AD/DA converter. The Labview
216 software (National Instruments) and a PCI-MIO-16E-4 I/O module were used for
217 generating and applying the potential program as well as for acquiring data, such as
218 current intensities.

219 Prior to electrochemical measurements, the solution **was** de-aerated with ultra-pure N₂ (U
220 Quality from Air Liquide) for 30 min, and a nitrogen stream **was** maintained over the
221 solution during the measurements in order to avoid any dissolved oxygen interferences.

222 The electrocatalytic activity of CME was investigated by using cyclic voltammetry (CV)
223 both in the absence and in the presence of the CR dye. In the CVs, the currents were
224 normalized with the geometrical surface area of the working electrode to provide more
225 useful correlations in terms of kinetic issues. Electrolysis at a constant potential (2 V) in
226 the presence of dye was carried out in the same electrolytic cell used for the CV studies.
227 The used **concentration** of the CR dye was 3.44×10^{-3} mmol (25 ppm) for CV studies and
228 6.88×10^{-3} mmol (50 ppm) for electrolysis in 0.10 M NaCl solution, at room temperature
229 without addition of hydrogen peroxide.

230

231 **2.5 Product analysis**

232 In order to quantify the extent of degradation of the organic pollutants by Fenton-like
233 reaction, after separation of the solid catalyst by centrifugation, an UV-vis
234 spectrophotometer (UV-2501PC from Shimadzu) was used at the characteristic
235 wavelengths $\lambda_{\max} = 427$ nm and 272 nm for Tar and Caf, respectively, in order to
236 determine the residual concentration of the pollutant in the reaction solution.

237 Liquid phase samples from electro Fenton-like reaction were analyzed by high
238 performance liquid chromatography (HPLC), equipped with an isocratic pump (Jasco
239 PU-980 Intelligent HPLC Pump) and a double on-line detection including an UV-vis
240 detector (Jasco Intelligent UV/vis detector). Separation of the different components was
241 carried out using the following HPLC ion exchange columns: IonPac AS11-HC from
242 Analytical, Aminex HPX-87 H ($\lambda=210$ and 260 nm) from Biorad, and RP18 from Merck
243 ($\lambda=497$ nm).

244 **The total organic carbon (TOC)** was determined using the NPOC method, with a
245 Shimadzu's Total Organic Carbon Analyzer TOC-L coupled with the ASI-L autosampler
246 of the same brand.

247

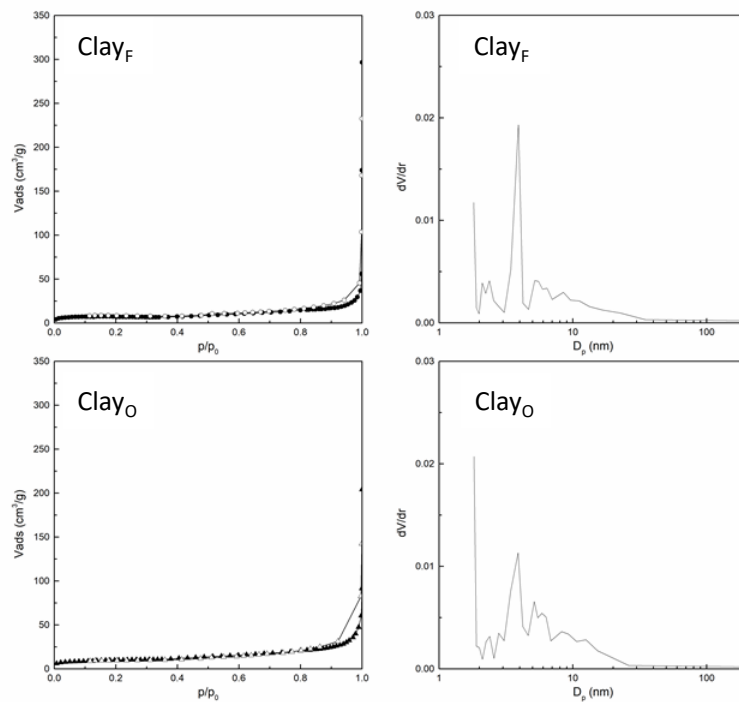
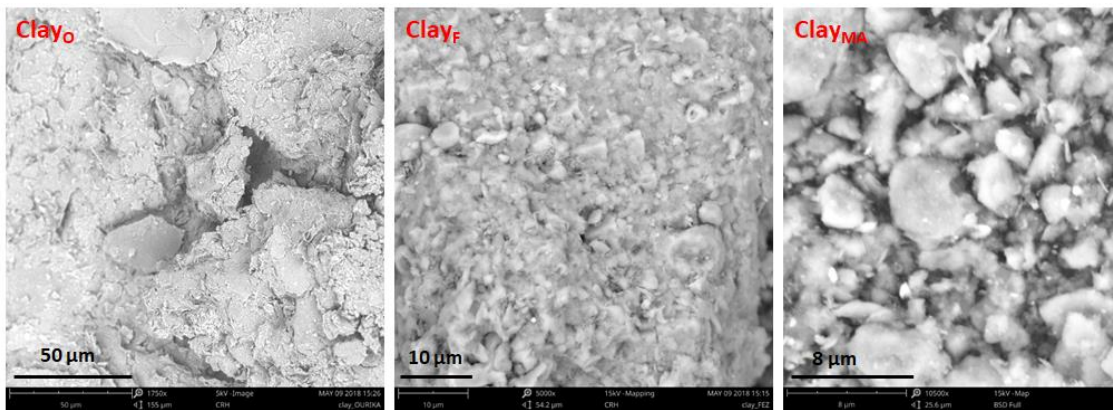
248 **3. Results and Discussion**

249 **3.1 Characterization of the heterogeneous clay catalysts**

250 Scanning electron microscopy (SEM) investigated the morphology of the raw clays, and
251 the textural properties were evaluated by N_2 adsorption analysis (Fig. 2). SEM images
252 obtained with different magnifications, show that the clays have a heterogeneous
253 morphology, with the presence of aggregates composed by particles of different size, with
254 Clay_{MA} having the smallest particles. Flat intercalated layers typical of the clay minerals
255 make some of these aggregates, especially in the case of Clay_O. From EDX spectra, the
256 amount of the typical elements of the clays are identified, Al, Si, Na, Mg, Fe, K, Mg, Ti
257 and Ca (Table S1). The presence of iron (Fe) with 7.46 wt% for Clay_O, 4.38 wt% for
258 Clay_F and 5.50 wt% for Clay_{MA}, makes these materials attractive for the Fenton reaction.
259 Furthermore, among the three types of clay, Clay_F possesses the highest calcium content
260 at 8.46 wt%, followed by Clay_{MA} with 2.40 wt%.

261 All clays exhibit an isotherm type IIb, according to the IUPAC (International Union of
262 Pure and Applied Chemistry) classification, with a hysteresis loop at high P/P^0 values,
263 typical for mesoporosity originating from interparticle voids (Bergaya, 1995; Klopogge,
264 2998; Weidler, 1997). Fig. 2B displays the N_2 -physisorption isotherms and the pore size
265 distribution curves of Clay_F and Clay_O, whereas those of Clay_{MA} were already reported
266 in a previous paper [Assila et al., 2023a]. The textural properties of all the pristine clays
267 are summarized in Table 1.

268



269 **Fig. 2.** A) SEM images and EDX spectra, and B) N₂ adsorption/desorption isotherms of
270 the pristine clays.

271

272 The specific surface areas calculated by the BET method are 22.5, 23.0, and 34.4 m²/g
273 for Clay_F, Clay_{MA} (Assila et al., 2023a), and Clay_O, respectively. Clay_O exhibits the
274 highest values of both S_{BET} and V_{total} (1.5 times greater than those of Clay_F). On the other
275 hand, although they have similar surface areas, Clay_{MA} has a significantly lower pore
276 volume than Clay_F.

277

278 **Table 1.** Textural properties of the pristine clays.

279

Samples	S _{BET} ^a (m ² /g)	V _{total} ^b (cm ³ /g)
Clay _F	22.5	0.060
Clay _{MA} (Assila et al., 2023a)	23.0	0.039
Clay _O	34.4	0.090

280 ^aSurface area calculated from the BET equation

281 ^bTotal pore volume determined from the amount adsorbed at $P/P_o = 0.99$

282

283 The distribution of the pore diameters was obtained using the BJH method based on a
284 discrete analysis of the adsorption branch of the isotherm, from which average pore
285 diameters equal to 3.8 and smaller than 6 or 18.6 nm were estimated for Clay_F, Clay_O and
286 Clay_{MA}, respectively.

287 These values confirm a mesoporous structure typical of the clays originated by
288 interparticle voids, and therefore depends on the properties of the formed aggregates,
289 which in turn depend on the properties of the particles that compose them. However, the
290 presence of particles with a broad size distribution could lead to the formation of an
291 irregular mesoporous structure, with a broad pore size distribution, which in turn

292 influences the surface area values. Moreover, the particular layered structure of clays
 293 should be considered. The assembly of clay platelets into successive structures (tactoids
 294 and aggregates) is affected by the clay mineral properties, in terms of platelet-platelet
 295 bonding energy, size, packing order, and alignment, leading to more or less rigid
 296 aggregates, also characterized by a different order degree (Bencheqroun et al., 2019a;
 297 Jiang et al., 2019; Moore and Reynolds, 1997).

298 Clay_{MA} was modified by introduction of copper or zinc in order to enhance the catalytic
 299 behavior of the pristine clay. The composition of all clays was determined by ICP-OES
 300 analysis, with Si, Al, and Fe as the most important elements. Ca, K, Ti, and Mg, typical
 301 elements of clay materials as well, were also quantified (Table 2).

302

303 **Table 2.** ICP-OES results (wt% of metals) of the pristine clays and the two
 304 metal-containing Clay_{MA} samples.

Sample	Si (wt%)	Al (wt%)	Na (wt%)	K (wt%)	Mg (wt%)	Ca (wt%)	Fe (wt%)	Cu (wt%)	Zn (wt%)	Ti (wt%)
Clay _{MA}	27.06	12.05	0.25	3.68	1.86	3.69	5.40	-	-	0.51
Cu-Clay _{MA}	27.60	11.35	0.28	2.61	0.58	0.23	4.55	0.43	-	0.43
Zn-Clay _{MA}	27.39	11.31	0.31	2.87	0.63	0.33	4.33	-	0.32	0.46
Clay _F	23.88	5.93	0.62	1.47	1.72	11.44	3.98	-	0.35	0.29
Clay _O	26.43	9.89	0.31	2.52	0.96	0.35	6.45	-	-	0.50

305

306 Clay_{MA} and Clay_O contain higher amounts of Fe (5.40 and 6.45 wt.%, respectively),
 307 whereas Clay_F is richer in calcium (11.44 wt.%), in agreement with EDX analysis. These
 308 differences in composition justifies the different colours of the clays (Fig. 1). The
 309 presence of iron in the pristine clays is expected to enhance the catalytic properties of
 310 these materials for Fenton reactions. Furthermore, the presence of various metals such as

311 copper (Cu), magnesium (Mg), zinc (Zn), and calcium (Ca) in the clays, along with iron,
 312 can induce the formation of hydroxyl radicals ($\cdot\text{OH}$) through the activation of hydrogen
 313 peroxide (H_2O_2), persulfate, and peroxymonosulfate. These reactions are known as
 314 Fenton-like processes.

315 In the case of Clay_{MA}, the introduction of Cu or Zn leads to a remarkable decrease in the
 316 Ca and Mg contents (about 90 and 70%, respectively); a more limited variation is instead
 317 observed for K, Fe, and Ti, whose contents decrease by about 20, 30, and 15%,
 318 respectively. The decrease in the content of the metals present in the original clay,
 319 especially observed for Ca and Mg, is reasonably due to an ion exchange process
 320 involving such cations and those contained in the aqueous solution of the Cu or Zn
 321 precursor nitrates (i.e., Cu^{2+} or Zn^{2+} , and H^+).

322 All these samples were analyzed by XPS to determine the composition, the relative
 323 distribution, and the oxidation state of the components present on the surface. In
 324 agreement with ICP-OES analysis, the predominant elements in all the recorded survey
 325 XPS resolution spectra are oxygen (O 1s), carbon (C 1s), iron (Fe 2p), silicon (Si 2p), and
 326 aluminum (Al 2s), typical for clay minerals (Elmi et al., 2016). In addition, small amounts
 327 of potassium (K 2p), calcium (Ca 2p), and sodium (Na 1s) were also detected. The binding
 328 energies (BE) of the principal elements as well as their surface amounts (wt%) are
 329 reported in Table 3.

330

331 **Table 3.** Binding energies (BE) and the amount of the elements (wt%) obtained from the
 332 XPS resolution spectra in the C 1s, O 1s, Cl 2p, N 1s and Ag 3d regions of the
 333 samples.

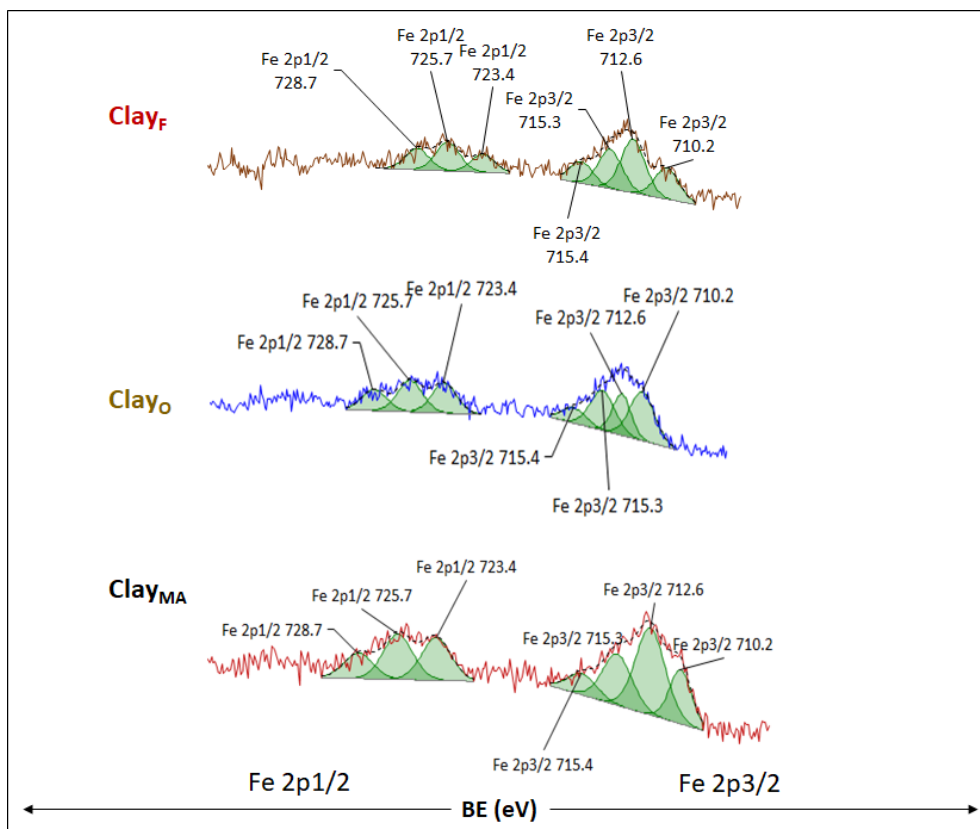
Sample	Clay _O		Clay _F		Clay _{MA}	
peak	BE (eV)	wt (%)	BE (eV)	wt (%)	BE (eV)	wt (%)

Si 2p	102.56	24.71	102.96	27.24	102.73	23.75
Al 2s	119.26	9.24	119.46	7.42	119.53	10.04
O 1s	531.76	50.59	532.06	51.33	532.03	49.96
C 1s	285.06	5.30	285.06	6.77	285.13	6.60
Fe 2p _{1/2}	724.36	1.96	725.76	1.72	725.83	1.37
Fe 2p _{3/2}	711.76	1.99	712.66	1.33	711.93	1.76
Fe 3p	56.14	2.03	56.25	1.01	55.91	1.58

334

335 It can be noted that the BE values are similar for all the elements irrespective of the
 336 pristine clay. By converse, some differences exist between the clays in the surface
 337 concentration of the different components, which are linked to the geological deposits
 338 where these materials came from. In particular, the surface amount of iron is in the order

339 Clay_O (5.98 wt%) > Clay_{MA} (4.71 wt%) > Clay_F (4.06 %). The comparison with the
 340 chemical analysis results (Table 2) shows similar Fe contents both on the surface and in
 341 the bulk, indicating that it is homogeneously distributed throughout the clays particles.
 342 **The energy separation (ΔE) between the two** peaks of Fe 2p is 12.6, 13.1 and 13.9 eV, for
 343 Clay_O, Clay_F and Clay_{MA}, respectively, and the presence of the Fe 3p peak suggests the
 344 existence of iron in different oxidation states. For all clay samples, the high-resolution
 345 XPS spectra **recorded** in the Fe region show that both **the 2p_{1/2} and 2p_{3/2} peaks visible** in
 346 the **corresponding** survey spectra can be deconvoluted in three and four components,
 347 respectively (Fig. 3).



348

349 **Fig. 3.** High-resolution XPS spectra of Fe 2p of all pristine clays.

350

351 For all the samples, the Fe 2p_{1/2} peak appears to be composed by three components at
 352 728.7, 725.7, and 723.4 eV, whereas the Fe 2p_{3/2} peak results from the overlapping of four
 353 contributions at BE values of 710.2, 712.6, 715.3, and 715.4 eV. These values of BE are
 354 related to the presence of Fe³⁺ and Fe²⁺ in the form of oxides in the clay minerals (Elmi
 355 et al., 2016; Handbook of X-ray Photoelectron Spectroscopy, 1992; Naumkin et al.,
 356 2012).

357 The C 1s peak at about 285 eV is ascribable to surface-atmosphere interactions or to
 358 residual precursors (Ihekweme et al., 2020; Todea et al., 2013), whereas the O 1s peak
 359 close to 532 eV is due to the elemental oxygen, oxides, oxygen in water, and metal oxides
 360 associated with the elements (Ihekweme et al., 2020). Signals of Si 2p at 103 eV and Al
 361 2s at 119.5 eV are attributed to Si-O-Si and Si-O-Al chemical bonds, or to both atoms
 362 coordinated with other elements, typical of these type of materials (Elmi et al., 2016;

363 Tissot et al., 2016). Both the Si 2p and Al 2s peaks can be deconvoluted in three
364 components, as shown in their high-resolution XPS spectra (Fig. S2). For Si 2p, the
365 presence of these three contribution in all clays suggests that Si atoms are tetrahedrally
366 coordinated with oxygen by Si-O-Si and Si-O-Al, which confirms the presence of such
367 bonds in these materials (Elmi et al., 2016). In addition to those of Al 2s, Al 2p peaks
368 were identified at about 74 eV for all the pristine clays. The presence of the three
369 components for the Al 2s signal and the appearance of the Al 2p peak close to 74 eV
370 suggest the existence of the same coordination than for Si and the presence of Al-OH
371 bonds where aluminum is in tetrahedral and octahedral coordination. From the literature,
372 the binding energy values of Al 2p in the simultaneous presence of tetrahedral and
373 octahedral Al atoms are intermediate between the binding energy values of octahedrally
374 and tetrahedrally coordinated species (Elmi et al., 2016). Thus, the BE values at 74.14,
375 73.25, and 74.91 eV for Clay_O, Clay_F, and Clay_{MA}, respectively, suggest that Al atoms at
376 the clays surface have tetrahedral or/and octahedral coordination (Fig. S2).

377 Samples obtained by modifying Clay_{MA} with Cu or Zn were also analyzed by XPS.
378 Concerning the major components, their XPS profiles were similar to that of the pristine
379 clay. The BE regions of Cu 2p and Zn 2p were also investigated to have information about
380 the nature and the surface concentration of the metals. Peaks of Cu 2p_{1/2} and Cu 2p_{3/2} were
381 detected at 953.48 eV and 931.98 eV, respectively, from which a Cu surface amount of
382 0.47 wt% was calculated. Likewise, in the XPS spectrum of Zn-Clay_{MA}, two peaks
383 ascribable to Zn 2p_{1/2} and Zn 2p_{3/2}, respectively, were identified at 1041.11 eV and
384 1025.21 eV, which allowed of determining a Zn surface content of 0.34 wt%.
385 Noteworthy, both the Cu and Zn concentrations on the surface are similar to those
386 determined by ICP-OES analysis for the bulk (Table 2), which suggests a homogeneous
387 distribution of the metals throughout the Clay_{MA} particles.

388 The XRD pattern of the raw clay from Fez (Clay_F) is presented to exemplify the
389 identification of the detrital and clay minerals present in these materials (Fig. S3). This
390 sample also contains non-clay minerals, typically detrital minerals like quartz, mica, and
391 plagioclase (< 2 mm). However, the presence of reflections at 3.86, 3.04, and 2.50 Å even
392 in the clay size fraction < 2 μm (oriented aggregates) indicates that calcite is the most
393 abundant non-clay mineral. Illite is indicated by the values for d₀₀₁ of 10.1 Å and d₀₀₂ of
394 5.02 Å, which are not influenced by EG-solvated conditions. Kaolin mineral, probably
395 kaolinite, was identified by the d₀₀₁ and d₀₀₂ reflections at 7.06 Å and 3.59 Å, respectively.
396 Moreover, chlorite is detected by the 00l reflections around 7.00 Å, 4.74 Å, and 3.55 Å
397 (Moore and Reynolds, 1997). Regarding smectite, it was identified combining the
398 patterns of air-dried samples with those of the glycolated and heated ones. Thus, the broad
399 reflection in the region of low-2θ, at 15.87 Å for the air-dried sample, is expanded to
400 approximately 17 Å for the EG-solvated. After heating, this peak collapses to 10 Å, which
401 is characteristic of the smectite mineral phase. Iron oxyhydroxide goethite is present in
402 trace amounts, as indicated by a weak, but typical reflection at 2.69-2.70 Å. As Clay_F,
403 Clay_O also contains illite and kaolin mineral, but the other phases are interstratified
404 vermiculite-chlorite, and goethite.

405

406 **3.2 Fenton-like reaction of the dyes**

407 The choice of the oxidation reaction is reliant on the nature of the pollutants and their
408 stability in Fenton-like reaction. The Fenton reaction is distinguished by the combination
409 of ferrous salts and hydrogen peroxide, culminating in the generation of hydroxyl radicals
410 (•OH) that swiftly drive the decomposition of pollutants (Assila et al., 2023a; Assila et
411 al., 2023b; Fu et al., 2022; Wang and Tang, 2021). Notably, clays contain a significant
412 iron content, which plays a crucial role in promoting degradation through the Fenton

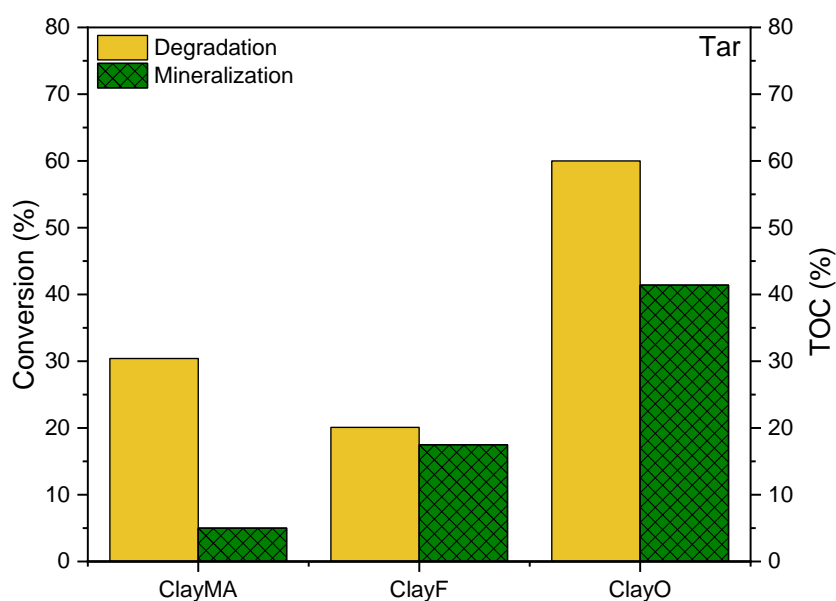
413 process. Furthermore, they also contain other cations that can facilitate the reaction (Table
414 2).

415 Concerning the pollutants, they were chosen due their presence in aqueous effluents in
416 Morocco. Congo Red (CR) and Tartrazine (Tar) are azo molecules, di and mono,
417 respectively, while caffeine (Caf) is a purine molecule based in an xanthine core with two
418 fused rings, a pyrimidinedione and imidazole, in which the three methyl groups are
419 located at positions 1, 3, and 7 (Fig. S4). Azo molecules are more easily oxidized than the
420 purine molecules by Fenton reaction (Assila et al., 2023a; Assila et al., 2023b; Fu et al.,
421 2022; Wang and Tang, 2021).

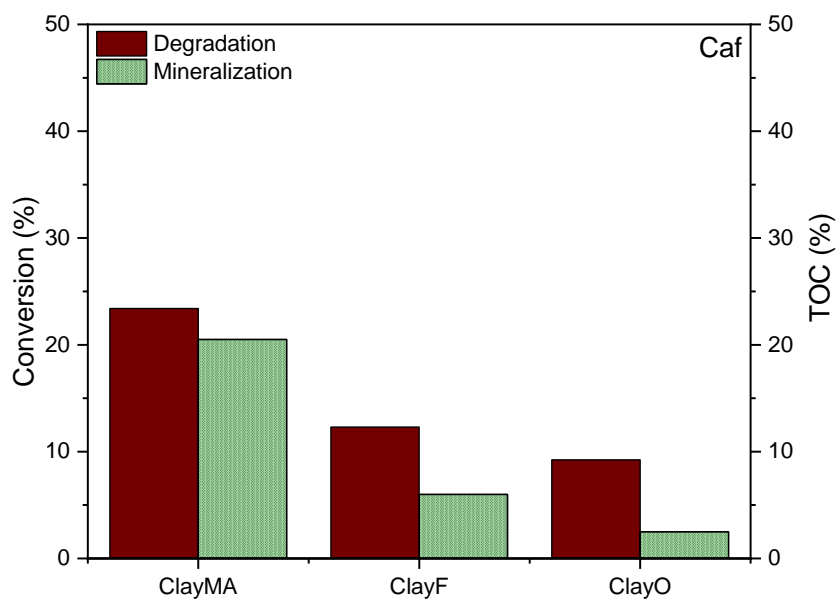
422 Tar and Caf were studied by a typical Fenton-like reaction with all the pristine clays.
423 Moreover, in order to improve the efficacy of the degradation of these pollutants, two
424 new heterogeneous catalysts were prepared with Clay_{MA} by the introduction of copper
425 (Cu-Clay_{MA}) or zinc (Zn-Clay_{MA}).

426 The catalytic results obtained with the different heterogeneous catalysts for the
427 degradation of Tar and Caf through Fenton-like reaction, using the experimental
428 conditions determined in (Assila et al., 2023a), are displayed in Fig. 4 and 5. Blank runs
429 were also made in the presence of only hydrogen peroxide or raw clays. Hydrogen
430 peroxide by itself was unable to degrade the dyes; indeed, only 4 % of conversion was
431 determined after 5 h of reaction. Similarly, the adsorption tests showed that the clays were
432 able to remove less than 3 % of the dyes after 5 h of reaction. These results suggest that
433 the simultaneous presence of H₂O₂ and clays is required to successfully remove dyes from
434 aqueous media through the Fenton-like reaction.

435 Fig. 4 displays the results for Tar and Caf degradation in terms of both pollutant's
436 conversion and TOC, after 5 h of reaction in the presence of the clay catalysts.



437



438

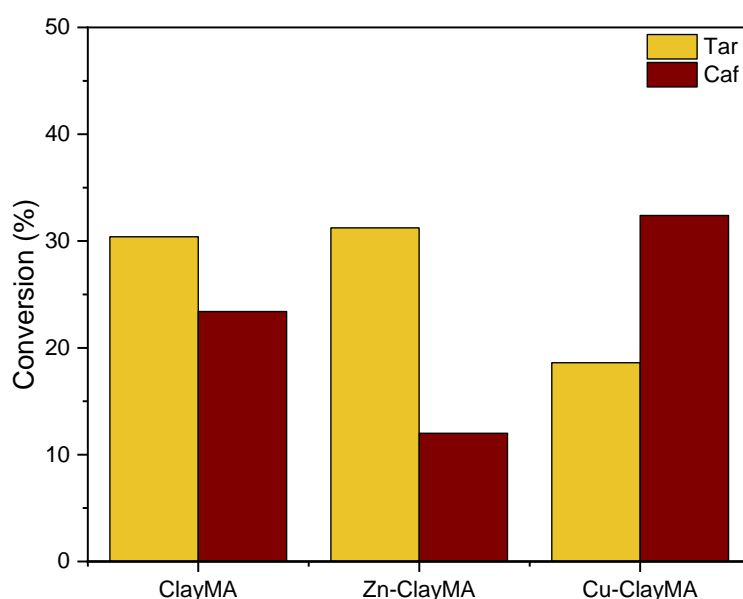
439 **Fig. 4.** Conversion and TOC percentages after Tar and Caf degradation by Fenton-like
 440 reaction in presence of Clay_{MA}, Clay_F, and Clay_O. Reaction conditions: 250 mL of dye
 441 solution (30 ppm); 5 mL of H₂O₂ solution (90 mM); T = 40 °C; pH = 3.0; 0.2 g of catalyst.

442

443 All clays are more effective in degrading Tar than Caf, with Clay_O showing the best
444 performance, achieving in the case of Tar 60 % of conversion and 41.5 % of
445 mineralization. This suggests that the catalyst can favor the formation of hydroxyl (\bullet OH)
446 radicals responsible for Tar degradation. On the other hand, Clay_{MA} and CLay_F show a
447 much lower removal capacity, reaching conversion values of 30.5 and 20.1 %,
448 respectively. Notably, although the conversion is higher for Clay_{MA}, the degree of
449 mineralization for this catalyst is only 5 %.

450 In the case of Caf degradation, the behavior of the clay catalysts are different, with Clay_{MA}
451 being the best one with 23.4 % of conversion. The low values obtained for Caf conversion
452 in the presence of the raw clays confirm that the caffeine molecule is very stable, and
453 these catalysts are not able to fully convert the pollutants initially present (30 ppm),
454 despite the better mineralization degree for Clay_{MA} (20.5 %), followed by Clay_F (6 %)
455 and Clay_O (2.5 %). These catalytic results are not only dependent on the molecular
456 structure of the pollutants but also to the chemical composition and the geological place
457 of the clays. For Tar degradation, a clay rich in iron at the surface (Clay_O, Fe = 5.98 wt%)
458 enhances the Fenton-like reaction (Clay_O), followed by Clay_F which has a homogeneous
459 distribution of iron with higher amount of calcium (Tables 2 and 3).

460 To investigate the effect of Zn or Cu addition on the catalytic behavior of Clay_{MA}, the
461 Fenton-like reaction was studied using both Zn-Clay_{MA} and Cu-Clay_{MA} as heterogeneous
462 catalysts for the removal of both dyes. The pertinent results are compared with those
463 obtained for the pristine clay in Fig. 5.



464

465 **Fig. 5.** Conversion of Tar and Caf by Fenton-like reaction in the presence of Clay_{MA}, Zn-
 466 Clay_{MA}, and Cu-Clay_{MA}. Reaction conditions: 250 mL of dye solution (30 ppm); 5 mL of
 467 H₂O₂ solution (90 mM); T = 40 °C; pH = 3.0; 0.2 g of catalyst.

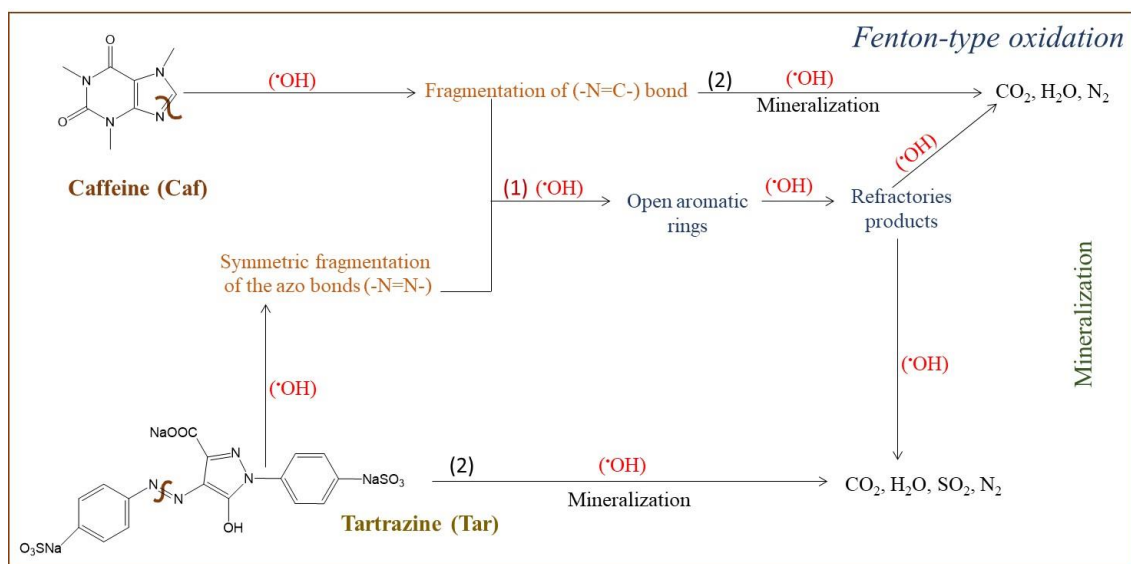
468

469 Zn-Clay_{MA} and Clay_{MA} have the same behavior for Tar conversion, which suggest that
 470 the presence of Zn does not improve its degradation. In addition, the presence of copper
 471 leads to worst performance. By converse, for Caf degradation the presence of copper
 472 improves the oxidation of the molecule (32.4 %) compared to the pristine clay, the pristine
 473 clay, whereas the presence of Zn is detrimental for the catalyst, which loses its activity.

474 From the catalytic results obtained for the Fenton-like reaction, the best catalysts turned
 475 out to be the raw clay from Ourika region (Clay_O) and the Cu-Clay_{MA} sample for Tar and
 476 Caf degradation, respectively.

477 The stability of Clay_O in the Fenton-like oxidation of Tar was studied by performing two
 478 reaction-regeneration cycles and the same catalytic behavior was observed. In addition,
 479 after each reaction test, the amount of leached metals was measured by ICP-OES and no

480 dissolution of metals was detected (within the experimental error) in all the experiments,
 481 indicating that the catalysts are stable under the experimental conditions used.
 482 Fenton reaction occurs between iron and H₂O₂ to generate highly oxidative hydroxyl
 483 radicals ([•]OH), which are efficient in degrading pollutants in water. However, in the
 484 heterogeneous Fenton reaction, Fe is stabilized within the material's structure and
 485 generates [•]OH without the precipitation of iron hydroxide. The presence of iron at the
 486 clays surface allows enhancing the heterogeneous Fenton catalysis. In addition, other
 487 metals as Cu, Mg, Zn, or Ca, identified in the clays, together with iron can trigger not
 488 only H₂O₂ but also persulfate and peroxymonosulfate to generate [•]OH, the latter of which
 489 are known as Fenton-like reactions (Bokare and Choi, 2014; Santos et al., 2021). Both
 490 pollutants are degraded by the attacks of the hydroxyl radicals ([•]OH) produce during the
 491 Fenton-like reaction. The catalytic degradation pathways of Tar and Caf in the presence
 492 of clays by Fenton-like reaction could be proposed and present in Fig 6.

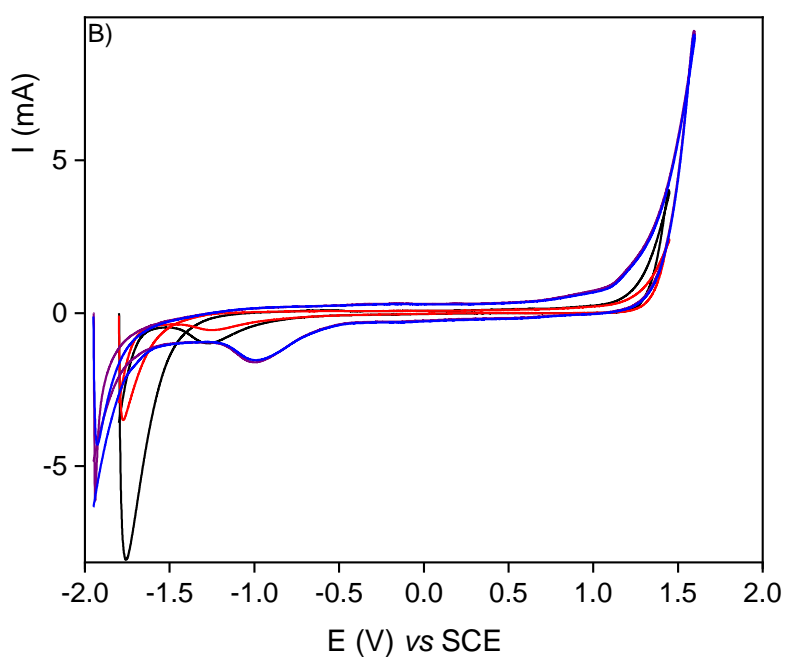
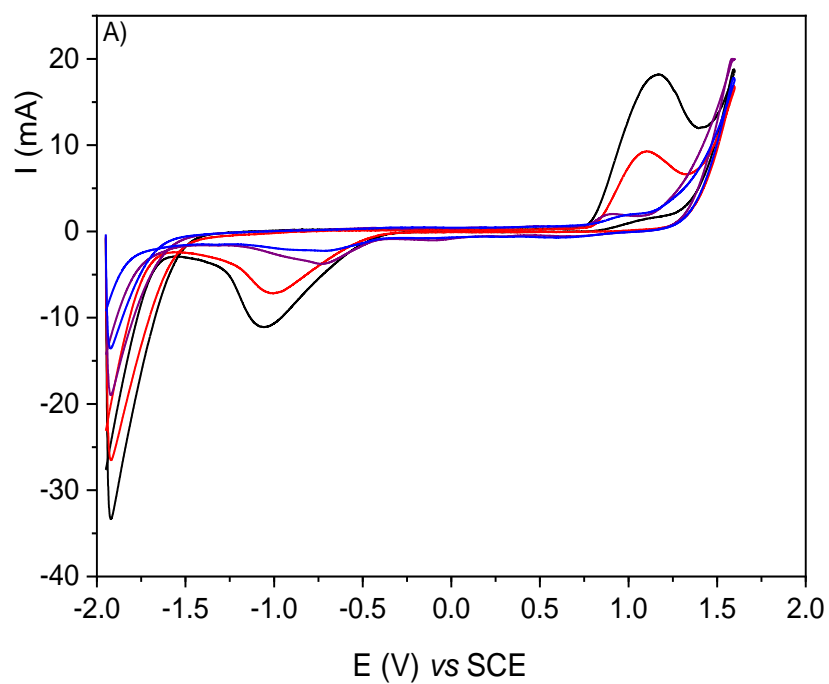


493
 494 **Fig. 6.** Proposed mechanism pathways for Fenton-like degradation of Caf and Tar
 495 molecules.
 496

497 The degradation of Tar molecule follows a symmetric degradation of the -N=N- azo bond,
498 since in the UV/vis spectrum, the band assigned at 260 nm disappears after 45 min of
499 reaction and the band at 427 nm decreases in intensity (Assila et al. 2023b). In the case
500 of Caf, which is a stable molecule, degradation could occur through the attack to the
501 aromatic rings in the -N=C- bond of the purine structure (Assila et al. 2023a). For both
502 pollutants, after the attack of the first radical the total opening of the aromatic rings
503 occurs, passing through the formation of low molecular weight organic acids (refractory
504 products) and finally reaching mineralization (pathway 1). The direct mineralization of
505 the pollutants seems to be more difficult, due to the presence of the refractories products
506 (pathway 2).

507 Being not stable in the acidic medium used in the Fenton-like reaction because of its
508 precipitation, the Congo red (CR) dye degradation was instead performed through the
509 electro Fenton-like reaction, using Clay_F and Clay_O modified electrodes. In our previous
510 work, CR was degraded using Fe-zeolite modified catalysts based on different zeolite
511 structures (Bencheqroun et al., 2022c). In that case, the Fe-(H)ZSM-5 modified catalysts
512 showed the best degradation results due to the acidic properties of the MFI structure
513 (Bencheqroun et al., 2022c).

514 The cyclic voltammometry studies between -2.0 V and +2.0 V vs. SCE potential with the
515 clay-modified electrodes based on Clay_O and Clay_F on Carbon Toray (CT) were
516 performed with a scan rate of 50 mVs⁻¹ in the presence of NaCl as electrolyte or with the
517 CR dye (25 ppm), at room temperature (Fig. 7).



518 **Fig. 7.** Cyclic voltammograms of the CME based on: A) Clay_F and B) Clay_O at a scan
 519 rate of 50 mVs⁻¹, in the absence of dye (black and red curves) and in the presence of 25
 520 ppm of CR (blue and violet curves) in NaCl (0.10 M).

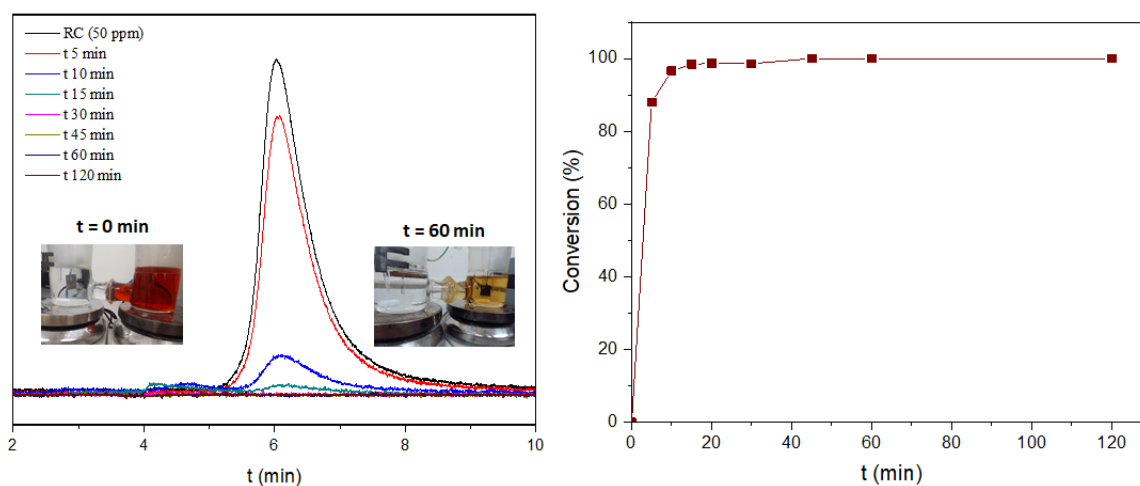
521

522 The electro behavior of the CME are different and it is probably related to the presence of
523 different iron species, *i.e.* the Fe(II)/Fe(III) couple, or other cations present on the surface
524 of both clays, as determined by ICP-OES and XPS analyses (Tables 2 and 3). The Clay_O-
525 modified electrode in the absence of CR dye (black and red curves) shows one irreversible
526 cathodic process at -1.3 V *vs.* SCE in 0.1 M NaCl medium. For the raw clay from Fez
527 City, an anodic redox process is observed at 1.2 V *vs.* SCE, and in the reverse scan of the
528 potential, a reduction peak can be seen at -1.0 V *vs.* SCE.

529 In the presence of CR dye (blue and violet curves), both CME are active and show an
530 increment in the anodic process, attributed to the catalytic activity of the catalysts. The
531 oxidation of CR starts at 0.8 V and 1.1 V *vs.* SCE for Clay_F and Clay_O, respectively, after
532 the oxidation of Fe(II) into Fe(III), indicating that the presence of Fe(III) species on the
533 electrode surface is necessary for the oxidation of this organic dye (Bencheqroun et al.,
534 2022c).

535 The rate-determining step of the CR oxidation process can be determined by voltammetry
536 studies, where the slope of the logI (mA) *vs.* v (mVs⁻¹) curves in 0.1 M NaCl medium
537 corresponds to 0.62 and 0.55 to Clay_F and Clay_O, respectively. These values are consistent
538 with a kinetic of the electrochemical reaction governed by the diffusion step
539 (Bencheqroun et al., 2022c).

540 The electrolysis of CR (50 ppm, 0.072 mM) with CME was performed with an applied
541 potential of 2.0 V *vs.* SCE, at room temperature, without hydrogen peroxide. Both clays-
542 CME are efficient in degrading the dye by electro Fenton-like reaction, but Clay_F is more
543 effective since it removes the dye in less time of reaction than Clay_O. Fig. 8 shows the
544 results obtained for Clay_F-modified electrode in the beginning and after 2 h of reaction,
545 as well as the evolution of the CR conversion.



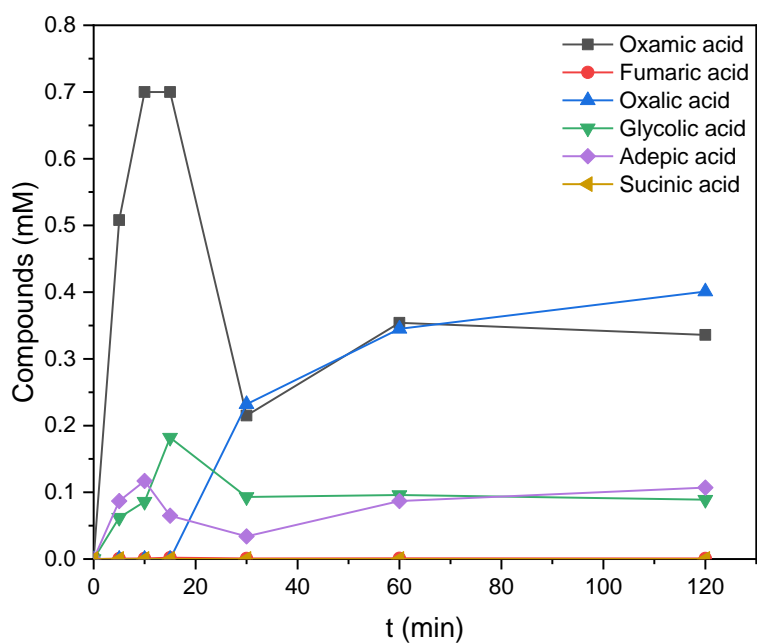
546

547 **Fig. 8.** HPLC-UV/vis chromatograms and the conversion of CR (■) vs. electrolysis time
 548 for the electrooxidation of CR in the presence of Clay_F-modified electrode.

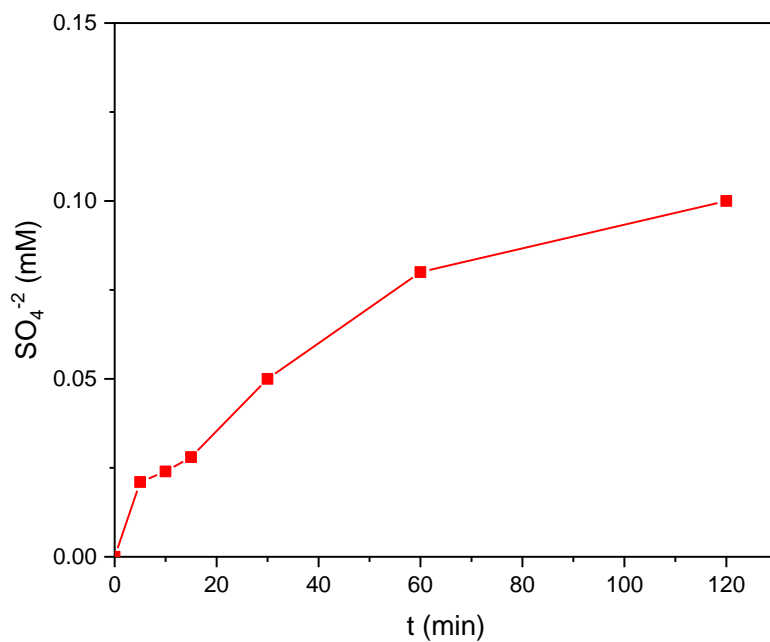
549

550 The results show that degradation occurs very fast since 81 % of the CR molecule is
 551 degraded after 5 min, being fully oxidized after 45 min of reaction (Fig. 8). At the end of
 552 reaction (2 h), TOC was determined and 67 % of mineralization was calculated. A similar
 553 value of mineralization (64 %) was previously obtained with the best Fe(H)ZSM5-
 554 modified electrode (Bencheqroun et al., 2022c). However, on the Clay_F-modified
 555 electrode, CR degradation appears to be faster than on the electrodes modified with Fe-
 556 MFI zeolites, on which only 74 % of conversion was achieved after 10 min of reaction
 557 (Bencheqroun et al., 2022c).

558 HPLC-UV/vis and **ionic chromatographic (IC)** analyses were employed to quantify the
 559 products at the end of reaction. The results reveal the presence of sulfate ions and several
 560 low molecular weight carboxylic acids, which are the byproducts of the CR rings opening
 561 triggered by the hydroxyl radicals produced during the electro-Fenton reaction (Fig. 9 and
 562 Table 4).



563

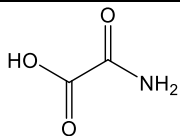
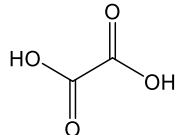
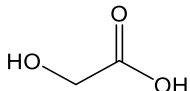
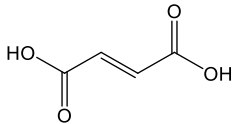
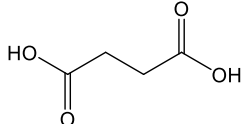
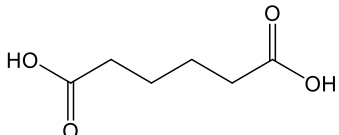


564

565 **Fig. 9.** The evolution of the compounds and sulfate ions during the electrolysis of CR in
 566 presence of CME based in Clay_F.

567

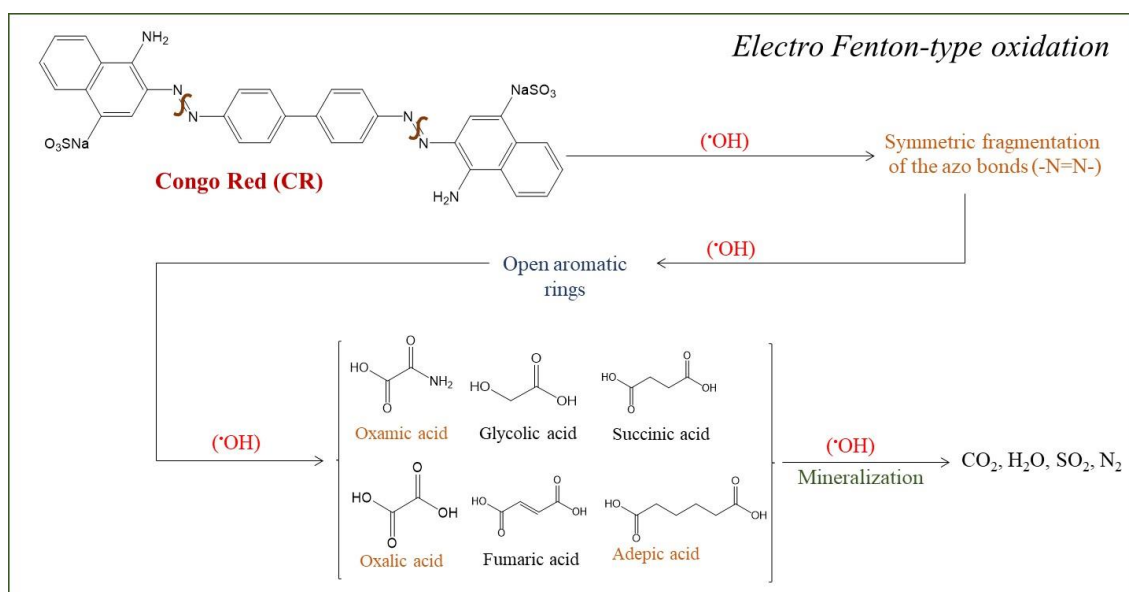
568 **Table 4.** Identification of the byproducts

Byproduct	Concentration (mM)	Percentage (%)	
Oxamic acid		0.336	36
Oxalic acid		0.401	43
Glycolic acid		0.089	9.5
Fumaric acid		0.011	<0.1
Succinic acid		0.5×10^{-5}	<0.01
Adipic acid		0.117	11.5

569

570 The major compounds identified at the end of electrolysis were oxamic, oxalic and adipic
571 acids, and sulfate ions. These recalcitrant products result from the degradation of the dye
572 by the electro-generation of the oxygenated radical species and the presence of Fe(III)-
573 hydroperoxo species. These species come from the oxidation of water in the adopted
574 oxidative conditions since oxygen is produced at 2.0 V vs. SCE (Bencheqroun et al.,
575 2022c). The higher mineralization rate (67 %) determined for Clay_F-CME is probably
576 related to the chemical composition of this raw clay as well as the geological place. As
577 mentioned before, this clay is rich in calcium and has a homogeneous distribution of iron,
578 which enhance the electro-Fenton reaction.

579 Based on our previous studies (Assila et al., 2023a; Assila et al., 2023b; Bencheqroun et
 580 al., 2022c), and on the identification of refractory products at the end of electrolysis, CR
 581 degradation can occur through the generation of oxygenated radical species, which
 582 facilitate the production of small organic acids and sulfate ions, and the successive
 583 mineralization of such organic species. The proposed mechanism pathway for CR by the
 584 electro-Fenton reaction is presented in Fig. 10.

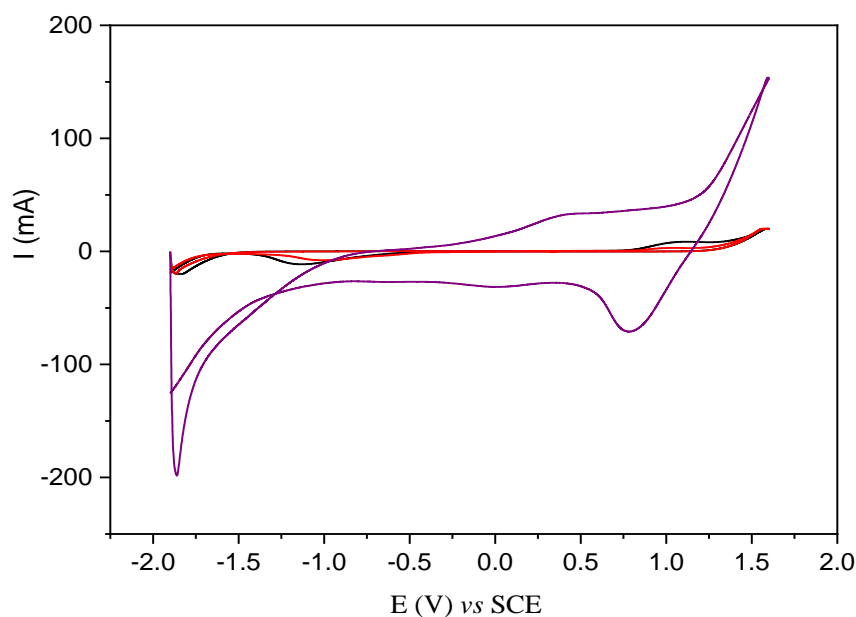


585

586 **Fig. 10.** Proposed mechanism pathway for electro-Fenton reaction of CR.

587

588 **Fig. 11** shows the cyclic voltammograms recorded before and after the electrolysis in the
 589 presence of CME modified with Clay_F.



590

591 **Fig. 11.** Cyclic voltammograms of CME based on Clay_F, recorded at 50 mVs⁻¹ before (red
 592 and black curves) and after the electrolysis (violet curve) of Congo Red dye (0.072 mM)
 593 in NaCl (0.10 molL⁻¹).

594

595 After electrolysis, an increase in the overall current intensities was observed, which is
 596 attributed to the restructuring of the electrode surface, including an increase in the active
 597 surface, due to the oxidative treatment during electrolysis. This increase may also be due
 598 to the contribution of current intensities resulting from the oxidation of some electrolysis
 599 products. **This behavior prove the stability of the CME based on Clay_F.** The same behavior
 600 was observed after the electrolysis of CR with zeolite.

601

602 **4. Conclusion**

603 In this study, the Fenton-like reaction was used as the oxidative process for
 604 degrading two organic pollutants (Tar and Caf), using three raw clays from Morocco as
 605 heterogeneous catalysts. Under the adopted experimental conditions, these clays are more

606 effective in oxidizing tartrazine than caffeine. The best catalytic results were obtained in
607 the presence of Clay_O and Clay_{MA}, with 60.0 and 23.4 % of conversion, and 41.0 and 20.5
608 % of mineralization for Tar and Caf, respectively. The introduction of zinc or copper into
609 Clay_{MA} does not lead to a significant improvement in the degradation of Tar, the
610 conversion of the metal-containing clay being equal to that of the starting one. However,
611 Cu-Clay_{MA} enhances the oxidation of the caffeine molecule (32.4 %) compared to the
612 pristine clay. Moreover, the electro-Fenton-like reaction was found to promote the
613 oxidation of CR at room temperature with a high mineralization degree (67 %), avoiding
614 the use of redox agents. Our study shows that the raw clays from Morocco can be
615 successfully applied in water treatments as a low-cost heterogeneous catalyst for a
616 sustainable process.

617

618 **Conflicts of interest**

619 There are no conflicts of interest to declare.

620

621 **Acknowledgments**

622 O.A. and Z.B. thank to ERASMUS+ Program for the mobility PhD grants. This research
623 work has been funded by national funds funded through FCT/MCTES (PIDDAC),
624 (Fundação para Ciência e Tecnologia, FCT) over the projects: LA/P/0045/2020 (ALiCE),
625 UIDB/50020/2020 and UIDP/50020/2020 (LSRE-LCM), Centre of Chemistry
626 (UID/QUI/0686/2020) and project BioTecNorte (operation NORTE-01-0145-FEDER-
627 000004), supported by the Northern Portugal Regional Operational Programme (NORTE
628 2020), under the Portugal 2020 Partnership Agreement, through the European Regional
629 Development Fund (ERDF).

630

631 **References**

- 632 Aid, A., Andrei R. D., Samira, A., Cammarano, C., Nibou, D., Vasile, H., Ni-exchanged
633 cationic clays as novel heterogeneous catalysts for selective ethylene oligomerization,
634 *Applied Clay Science*, 2017, 146, 432-438.
- 635 Anastas P.T., Zimmerman J.B., *The Molecular Basis of Sustainability*, Chem., 20161,
636 10–12, <http://dx.doi.org/10.1016/j.chempr.2016.06.016>
- 637 Antonelli, R., Malpass, G.R.P., da Silva, M.G.C., Vieira, M.G.A., Adsorption of
638 ciprofloxacin onto thermally modified bentonite clay: experimental design,
639 characterization, and adsorbent regeneration. *J. Environ. Chem. Eng.* 2020, 8, 104553.
- 640 Assila, O., Barros, Ó., Fonseca, A.M., Parpot, P., Soares, O.S.G.P., Pereira, M.F.R.,
641 Zerrouq, F., Kherbeche, A., Rombi, E., Tavares, T., Neves, I.C. Degradation of
642 pollutants in water by Fenton-like oxidation over LaFe-catalysts: Optimization by
643 experimental design, *Microporous and Mesoporous Materials*, 2023a, 3491, 112422,
644 DOI:10.1016/j.micromeso.2022.112422.
- 645 Assila, O., Vilaça, N., Bertão, A.R., Fonseca, A.M., Parpot, P., Soares, O.S.G.P., Pereira,
646 M.F.R., Baltazar, F., Bañobre-López, M., Neves, I.C. Optimization of iron-ZIF-8
647 catalysts for degradation of tartrazine in water by Fenton-like reaction, *Chemosphere*,
648 339, 2023b, 139634. doi.org/10.1016/j.chemosphere.2023.139634.
- 649 Axon S., James D., *The UN Sustainable Development Goals: How can sustainable*
650 *chemistry contribute? A view from the chemical industry*, *Curr. Opin. Green Sustain.*
651 *Chem.* 2018, 13, 140–145. <https://doi.org/10.1016/j.cogsc.2018.04.010>.
- 652 Bencheqroun, Z., Mrabet, I.El, Kachabi, M., Nawdali, M., Valdés, H., Neves, I., Zaitan,
653 H., Removal of basic and acid dyes from aqueous solutions using cone powder from
654 Moroccan cypress *Cupressus sempervirens* as a natural adsorbent, *Desalination and*
655 *Water Treatment*, 2019a, 166, 387–398., <https://doi.org/10.5004/dwt.2019.24514>
- 656 Bencheqroun, Z., Mrabet, I.El, Kachabi, M., Nawdali, M., Neves, I., Zaitan, H. Removal
657 of Basic Dyes from Aqueous Solutions by Adsorption onto Moroccan Clay (Fez City),
658 *Mediterranean Journal of Chemistry* 2019b, 8(2), 158-167
- 659 Bencheqroun, Z., Sahin, N.E., Soares, O.S.G.P., Pereira, M.F.R., Zaitan, H., Nawdali,
660 M., Rombi, E., Fonseca, A.M., Parpot, P., Neves, I.C. Fe(III)-exchanged zeolites as
661 efficient electrocatalysts for Fenton-like oxidation of dyes in aqueous phase, *Journal*

662 of Environmental Chemical Engineering 2022c, 10, 107891.
663 <https://doi.org/10.1016/j.jece.2022.107891>.

664 Bergaya, F. The meaning of surface area and porosity measurements of clays and pillared
665 clays, *J. Porous Mater.* 1995, 2, 91–96.

666 **Bokare, A. D., Choi, W. Review of Iron-free Fenton-like Systems for Activating H₂O₂ in
667 Advanced Oxidation Processes. *J. Hazard. Mater.* 2014, 275, 121-135.**

668 Brillas, E., Sires, I., Oturan, M.A. Electro-Fenton process and related electrochemical
669 technologies based on Fenton's reaction chemistry. *Chem. Rev.* 2009, 109, 6570-6631.

670 Chaplin, B.P., 2014. Critical review of electrochemical advanced oxidation processes for
671 water treatment applications. *Environ. Sci. Process. Impacts* 16, 1182-1203.

672 Elmi, C., Guggenheim, S., Giere, R., Surface crystal chemistry of phyllosilicates using
673 X-ray photoelectron spectroscopy: a review. *Clay Clay Miner.* 2016, 64 (5), 537–551

674 Ferreira, M., Biernacka, I. K., Fonseca, A.M., Neves, I.C., Soares, O.S.G.P., Pereira,
675 M.F.R., Figueiredo, J.L., Parpot, P. Study of the Electroreactivity of Amoxicillin on
676 Carbon Nanotube-Supported Metal Electrodes, *ChemCatChem* 2018, 10, 4900– 4909.

677 Fida, H.; Zhang, G.; Guo, S.; Naeem, A. Heterogeneous Fenton Degradation of Organic
678 Dyes in Batch and Fixed Bed Using La-Fe Montmorillonite as Catalyst. *J. Colloid
679 Interface Sci.* 2017, 490, 859–868, doi:10.1016/j.jcis.2016.11.085.

680 Fu, W., Yi, J., Cheng, M., Liu, Y., Zhang, G., Li, L., Du, L., Li, B., Wang, G., Yang, X.,
681 When bimetallic oxides and their complexes meet Fenton-like process, *J. Hazard.
682 Mater.*, 2022, 424, 127419, doi.org/10.1016/j.jhazmat.2021.127419;

683 Garrido-Ramírez, E.G., Mora, M.L., Marco, J.F., Ureta-Zanartu, M.S., Characterization
684 of nanostructured allophane clays and their use as support of iron species in a
685 heterogeneous electro-Fenton system. *Appl. Clay Sci.* 2013, 86, 153-161.

686 **Haciosmanoglu, G.G., Mejías, C., Martín, J., Santos, J.L, Aparicio, I., Alonso, E.,
687 Antibiotic adsorption by natural and modified clay minerals as designer adsorbents for
688 wastewater treatment: A comprehensive review. *Journal of Environmental
689 Management*, 2022, 317, 115397.**

690 Hadjltaief, H.B., Galvez, M.E., Zina, M.B., Costa, P., TiO₂/clay as a heterogeneous
691 catalyst in photocatalytic/photochemical oxidation of anionic reactive blue 19,
692 *Arabian Journal of Chemistry*, 2019, 12 (7), 1454-1462

693 Handbook of X-ray Photoelectron Spectroscopy: A Reference Book of Standard Spectra
694 for Identification and Interpretation of XPS Data, ed. Jill Chastain, Physical
695 Electronics Division, Perkin-Elmer Corporation, 1992.

696 Herney-Ramirez, J., Vicente, M.A., Madeira, L.M., Heterogeneous photo-Fenton
697 oxidation with pillared clay-based catalysts for wastewater treatment: a review. *Appl.*
698 *Catal. B Environ.* 2010, 98, 10-26.

699 Ihekwe, G.O., Shondo, J.N., Orisekeh, K.I., Kalu-Uka, G.M., Nwuzor, I.C., Onwualu,
700 A.P. Characterization of certain Nigerian clay minerals for water purification and other
701 industrial applications, *Heliyon* 2020, 6, 03783.

702 Jiang, J.Q., Ashekuzzaman, S.M., Hargreaves, J.S.J., Mcfarlane, A.R., Badruzzaman,
703 A.B.M., Tarek, M.H. Removal of arsenic (III) from groundwater applying a reusable
704 Mg-Fe-Cl layered double hydroxide, *J. Chem. Technol. Biotechnol.* 90 (2015) 1160–
705 1166; *Mediterranean Journal of Chemistry* **2019**, 8(2), 158-167.

706 Jesus, J.H.F., Lima, K.V.L., Nogueira, R.F.P., Copper-containing magnetite supported on
707 natural clay as a catalyst for heterogeneous photo-Fenton degradation of antibiotics in
708 WWTP effluent, *Journal of Environmental Chemical Engineering*, 2022, 10 (3)
709 107765.

710 Klopogge, J.T. Synthesis of smectites and porous pillared clay catalysts: a review, *J.*
711 *Porous Mater.* 1998, 5, 5–41.

712 Liu, Y., Zhao, Y., Wang, J., Fenton/Fenton-like processes with in-situ production of
713 hydrogen peroxide/hydroxyl radical for degradation of emerging contaminants:
714 Advances and prospects, *J. Hazard. Mater.*, 2021, 404, 124191,
715 doi.org/10.1016/j.jhazmat.2020.124191;

716 Ma, H., Zhuo, Q., Wang, B. Electro-catalytic degradation of methylene blue wastewater
717 assisted by Fe₂O₃-modified kaolin. *Chem. Eng. J.*, 2009, 155, 248e253.

718 Maryan, A.S., Montazer, M., Damerchely, R., Discoloration of denim garment with color
719 free effluent using montmorillonite based nano clay and enzymes: nano bio-treatment
720 on denim garment, 2015, 91, 208-215.

721 **Moore, D.M. and Reynolds, R.C. X-ray diffraction and identification and analysis of clay**
722 **minerals, 1997, 2nd Edition, Oxford University Press, New York.**

723 Naumkin, A.V., Kraut-Vass, A., Gaarenstroom, S.W., Powell, C.J. NIST X-ray
724 Photoelectron Spectroscopy Database, NIST Standard Reference Database 20,
725 Version 4.1, Last Update to Data Content: 2012, <http://dx.doi.org/10.18434/T4T88K>;

726 Ozcan, A., Ozcan, A.A., Demirci, Y., Sener, E. Preparation of Fe₂O₃ modified kaolin and
727 application in heterogeneous electro-catalytic oxidation of enoxacin., Appl. Catal. B
728 Environ. 2017, 200, 361-371

729 Poza-Nogueiras, V., Rosales, E., Pazos, M., Sanrom, M.A. Current advances and trends
730 in electro-Fenton process using heterogeneous catalysts e A review, Chemosphere,
731 2018, 201, 399-416.

732 Santos, B.L.C., Parpot, P., Soares, O.S.G.P., Pereira, M.F.R., Rombi, E., Fonseca, A.M.,
733 Neves, I.C. Fenton-Like Bimetallic Catalysts for Degradation of Dyes in Aqueous
734 Solutions, Catalysts 2021, 11, 32. <https://doi.org/10.3390/catal11010032>

735 Schoonheydt R.A., Clays: from two to three dimensions, in Introduction to zeolite science
736 and practice, H. van Bekkum, E.M. Flanigen, J.C. Jansen (Eds.), Studies in Surface
737 Science and Catalysis, Elsevier, Netherlands, V. 58, 1991, pp 201-239.

738 Tissot, H., Li, L., Shaikhutdinov, S., Freund, H.J. Preparation and structure of Fe
739 containing aluminosilicate thin films. Phys. Chem. Chem. Phys. 2016, 18 (36), 25027–
740 25035;

741 Todea, M., Vanea, E., Bran, S., Berce, P., Simon, S., XPS analysis of aluminosilicate
742 microspheres bioactivity tested in vitro. Appl. Surf. Sci. 2013, 270, 777–783.

743 United Nations, 2023, [https://www.un.org/sustainabledevelopment/wp-](https://www.un.org/sustainabledevelopment/wp-content/uploads/2019/07/UN-SG-Roadmap-Financing-the-SDGs-July-2019.pdf)
744 [content/uploads/2019/07/UN-SG-Roadmap-Financing-the-SDGs-July-2019.pdf](https://www.un.org/sustainabledevelopment/wp-content/uploads/2019/07/UN-SG-Roadmap-Financing-the-SDGs-July-2019.pdf)

745 United Nations, Sustainable development knowledge platform, sustainable development
746 goals, 2016. <https://sustainabledevelopment.un.org/sdgs>

747 Usman, M., Monfort, O., Gowrisankaran, S., Hameed, B.H., Hanna, K., Al-Abri, M. Dual
748 functional materials capable of integrating adsorption and Fenton-based oxidation
749 processes for highly efficient removal of pharmaceutical contaminants, Journal of

750 Water Process Engineering, 2023, 52, 103566.
751 <https://doi.org/10.1016/j.jwpe.2023.103566>.

752 Wang, J.; Tang, J. Fe-based Fenton-like catalysts for water treatment: Preparation,
753 characterization and modification, Chemosphere, 2021, 276, 130177,
754 doi.org/10.1016/j.chemosphere.2021.130177.

755 Weidler, P.G. BET sample pretreatment of synthetic ferrihydrite and its influence on the
756 determination of surface area and porosity, J. Porous Mater. 1997, 4, 165–169.

757

758